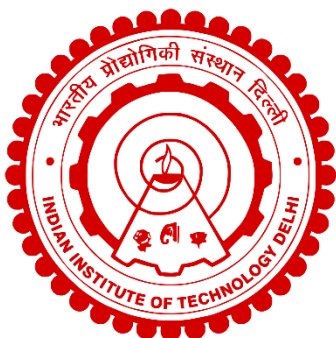


**SYNTHESIS, STRUCTURAL, GAS SENSING, IN-SITU  
XPS AND KPFM INVESTIGATION OF PLD GROWN 2D  
MATERIALS BASED NANOSTRUCTURES**

**Prashant Bisht**



**DEPARTMENT OF PHYSICS**

**INDIAN INSTITUTE OF TECHNOLOGY DELHI**

**JULY 2023**

**SYNTHESIS, STRUCTURAL, GAS SENSING, IN-SITU  
XPS AND KPFM INVESTIGATION OF PLD GROWN 2D  
MATERIALS BASED NANOSTRUCTURES**

by

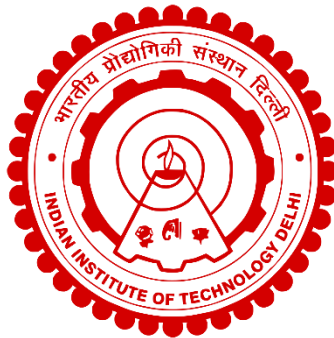
**Prashant Bisht**

Department of Physics

*Submitted*

*in fulfilment of requirements of degree of Doctor of Philosophy*

*to the*



**INDIAN INSTITUTE OF TECHNOLOGY DELHI**

©Indian Institute of Technology Delhi (IITD), New Delhi, 2023

## **Dedication**

This dissertation is dedicated to my parents Mr. Santan Singh and Mrs. Poonam Bisht. Their support, blessings, encouragement, and constant love have sustained me throughout my life.

# CERTIFICATE

I am satisfied that the thesis entitled “**Synthesis, structural, gas sensing, In-situ XPS and KPFM investigation of PLD grown 2D materials-based nanostructures**” submitted by Mr. Prashant Bisht is worthy of consideration for the award of the degree of **Doctor of Philosophy** and is a record of original and bonafide research work carried out by him under our supervision. The results contained in it have not been submitted in part or full to any other university or institute for the award of any degree/diploma.

**Prof. B. R. Mehta**

Department of Physics  
Indian Institute of Technology Delhi  
New Delhi-110016, India

**Prof J.P Singh**

Department of Physics  
Indian Institute of Technology Delhi  
New Delhi-110016, India

Date: 26<sup>th</sup> July 2023

## **ACKNOWLEDGEMENTS**

---

*The journey of this doctoral thesis might have been a fond illusion without the contribution and support from many inspiring individuals that create a productive environment for me to work in. Therefore, I would like to express my sincere gratitude to all the people who contributed to forming such a stimulating atmosphere that helped me over the years to complete my work successfully.*

*Firstly, I wish to acknowledge my sincere gratitude towards my thesis supervisor **Prof. B. R. Mehta**, who contributed significantly to shaping and guiding the direction for my thesis work. I am profoundly grateful to him for providing me with an environment where I learned from his knowledge, experience and wisdom that enabled me to complete this study. He has always inspired me with his endless patience, in-depth knowledge, and dedication to accomplish tasks at stipulated time. The allegiance with which he handles such a large group and is always willing to give new ideas and implement them is highly motivational. I would also like to express my thanks to **Dr. Poonam Mehta**. She has always motivated me and given moral support in the most caring way during my thesis work.*

*I am highly obliged to my co-supervisor **Prof J.P Singh** for the valued support and suggestions which helped me in consolidation and realization of this work.*

*Besides my supervisors, I sincerely thank and appreciate the efforts of the SRC members, **Prof. Pankaj Srivastava**, **Prof. Rajendra Singh**, and **Prof. Pravin P Ingole**, for their ever-helping approach and supportive nature.*

*I am thankful to **Prof. Ratan Mala Chatterjee, and Prof. Pankaj Srivastava**, Head of the Department, Physics, IIT Delhi, for providing necessary facilities.*

*I feel fortunate to be associated with Thin Film Lab, which brings along an immense history of research and a tradition of dedication and innovation. I would also like to thank **Dr. Deepak Varandani, Dr. Khushboo Agarwal, Dr. Dipika Sharma, Dr. Vinod Poonia, Dr. Rishabh Sharma, Dr. Arvind, Dr. Nisha Kodan, Dr. Vishakha Kaushik, Mr Abhishek Ghosh and Ms Narinder Kaur** from whom I learned my things. I wish to extend a word of thanks to **Mr Saurabh Singh and Mr B.R. Khatri**, who helped me in technical and non-technical aspects of research. I am much obliged to be associated with such a large and helping colleagues at a thin film laboratory.*

*I feel privileged to work with **Dr. Branson Belle, Dr. Ayaz Ali, Dr. Ozhan Kyobasi, Dr. Ingvild, Dr. Martin and Dr. Per Erik Vullum, from SINTEF Norway** who performed many experiments along with me and provided valuable suggestions on writing and understanding many aspects of research. I thank them for their meticulous and patient effort in enriching the quality of my research work.*

*I wish to extend heartfelt thanks to **Ms Pallavi Aggarwal and Mr Abhishek Ghosh** for being by my side during the peak time of my experimental work. Their friendship and support were a great source of encouragement and have spent the most enlightening time of my research life. I sincerely thank and*

*acknowledge the useful comments and insightful discussions that have helped me throughout my doctorate journey.*

*I am delighted to express my sincere appreciation to **my family** for their love, support and understanding that allowed me to nurture my dream and keep looking forward to more exceptional achievements in the future. I am incredibly grateful to my siblings **Sushant Bisht, Aditi Bisht** and **Kashvi Bisht** who encouraged and helped me at every stage of my personal and academic life and longed to see this achievement come true.*

*I gratefully acknowledge the University grant commission (UGC) for providing the funding support and Senior Research Fellowship for this study.*

*Above all, I owe it all to Almighty God for granting me the wisdom, health, and strength to complete this task and enabling me to compile it.*

**Prashant Bisht**

**Date:** 26-07-2023

**Place:** New Delhi

## ABSTRACT

---

Two dimensional layered materials with atomic scale thickness and layered structure have gained substantial research interest due to their fascinating properties like high specific area, tunable bandgap, strong coulomb interaction, and ease of making heterostructures at atomic thickness. This makes them suitable materials for various application in electronics, photonics and desirable for interdisciplinary research fields like catalysis, sensors, biosensors, neuromorphic computing, renewable energy etc. However, adoption of these materials for practical application requires an extensive understanding of their physical and chemical properties. Also, scalable synthesis of 2D materials with precise control over the growth is a major challenge.

In the present study, pulsed laser deposition (PLD) technique was used to synthesize high quality, large area, few layered thin films of MoO<sub>3</sub>, WS<sub>2</sub>, and SnS. These materials belong to three distinct families of 2D materials, namely transition metal oxide, transition metal di and mono chalcogenides. Gas sensing properties of these films were studied to understand and achieve highly selective sensor at low operating temperature with limit of detection in parts per billion (ppb).

Synthesis of  $\alpha$ -MoO<sub>3</sub> layered thin film of varying thickness of 6, 18 and 70 nm was achieved through PLD. All the growth parameters were optimized, and the three distinct thicknesses were obtained by changing the number of laser pulse. X-ray diffraction (XRD) and Raman spectroscopy confirmed the

formation of anisotropic  $\alpha$ -MoO<sub>3</sub>. Atomic force microscopy (AFM) images showed the evolution of morphology from 2D layers to oriented crystallite growth with increase in film thickness. X-ray photoelectron spectroscopy (XPS) measurements depicted higher concentration of oxygen vacancies in 70 nm thin film sample and higher oxygen adsorption in 6nm thick 2D layered sample. Thickness dependent gas sensing behaviour was studied towards NO<sub>2</sub> gas. 2D layered sample showed highest response of about 25 % at lower temperature (100 °C). It also exhibited lower detection limits (100 ppb) and selectivity towards NO<sub>2</sub> gas. Comparatively, TF showed poor response (4%) towards NO<sub>2</sub> at 100 °C but got increased gradually to 35% at 250 °C indicating higher diffusion of analyte gas due to its higher thickness. A change from n-type to p-type gas sensing response was observed with decreasing thickness of the  $\alpha$ -MoO<sub>3</sub> films which might be attributed to the increased surface adsorption and higher Schottky barrier at metal-MoO<sub>3</sub> junction in sample with lower thickness.

Synthesis of vertically and horizontally oriented WS<sub>2</sub> layered films was achieved by varying the PLD parameters. The samples grown with a combination of lower temperature (400 °C) and higher pressure (70 mTorr) exhibited a vertical flake-like growth, with a flake thickness of ~ 2-5 nm. However, at higher temperatures (600 °C) and lower pressure (30 mTorr), planar film growth was obtained. XRD, Raman spectra and XPS spectra confirmed 2H semiconducting phase and high film quality. Whereas FESEM, AFM and cross-sectional transmission electron microscopy (TEM) measurements were utilized to elucidate the growth mechanism. Further,

vertically oriented films showed the best response with selectivity towards NO<sub>2</sub> at room temperature (RT) with limit of detection less than 50 ppb. On the contrary, subdued response was obtained in the case of planar films. The results showed a large dependence of the gas sensing mechanism and parameters on layer orientation, and the crucial role of edge sites.

Synthesis of high quality and ultrathin SnS thin film was achieved via PLD followed by the decoration of noble metal nanoparticles (Ag, Au, and Pd) using gas phase synthesis technique. Growth of SnS film was optimized by varying the growth temperature between RT to 500 °C. Gas sensing measurements were performed on pristine and metal nanoparticle decorated SnS films to tune the response and selectivity.

To further understand the gas sensing mechanism, In-situ gas sensing techniques were employed to further explore the sensing mechanism in detail. Near ambient pressure (NAP) XPS measurements were performed on α-MoO<sub>3</sub> thin films to study the effect of film thickness, morphology, and defects towards NO<sub>2</sub> gas sensing by analysing the change in position and intensity of Mo 3d peak. In-situ Kelvin probe force microscopy (KPFM) was performed on pristine, Ag, and Pd nanoparticle decorated SnS film. In-situ KPFM mapped local changes in the work function of film due to analyte gas. The effect of Ag to enhance NO<sub>2</sub> response and Pd to increase selectivity towards H<sub>2</sub> gas has been manifested from the change in surface potential and work function. These results open opportunities to explore PLD as a potential synthesis technique for 2D materials and give a unique perspective to their applications as gas sensors.

## सार

परमाणु पैमाने की मोटाई और स्तरित संरचना के साथ २ डायमेंशनल (2D) स्तरित सामग्री ने अपने आकर्षक गुणों जैसे उच्च विशिष्ट क्षेत्र, ट्यून करने योग्य बैंडगैप, मजबूत कूलम्ब इंटरैक्शन और परमाणु मोटाई पर हेटरोस्ट्रक्चर बनाने में आसानी के कारण पर्याप्त अनुसंधान रुचि प्राप्त की है। यह उन्हें इलेक्ट्रॉनिक्स, फोटोनिक्स में विभिन्न अनुप्रयोगों के लिए उपयुक्त सामग्री बनाता है और अंतःविषय अनुसंधान क्षेत्रों जैसे कटैलिसिस, सेंसर, बायोसेंसर, न्यूरोमॉर्फिक कंप्यूटिंग, नवीकरणीय ऊर्जा आदि के लिए वांछनीय है। हालांकि, व्यावहारिक अनुप्रयोग के लिए इन सामग्रियों को अपनाने के लिए उनके भौतिक और रासायनिक गुणों की व्यापक समझ की आवश्यकता होती है। इसके अलावा, विकास पर सटीक नियंत्रण के साथ 2D सामग्री का स्केलेबल संश्लेषण एक बड़ी चुनौती है।

वर्तमान अध्ययन में, धातु  $\text{MoO}_3$ ,  $\text{WS}_2$ , और  $\text{SnS}$  की उच्च गुणवत्ता, बड़े क्षेत्र, कुछ स्तरित पतली फिल्मों को संश्लेषित करने के लिए पल्सड लेजर डिपोजिशन (PLD) तकनीक का उपयोग किया गया था। ये सामग्रियां 2D सामग्रियों के तीन अलग-अलग परिवारों से संबंधित हैं, अर्थात् संक्रमण धातु ऑक्साइड, संक्रमण धातु डाय और मोनो चालकोजिनाइड्स। इन फिल्मों के गैस सेंसिंग गुणों का अध्ययन भागों प्रति बिलियन (ppb) में पता लगाने की सीमा के साथ कम ऑपरेटिंग तापमान पर अत्यधिक चयनात्मक सेंसर को समझने और प्राप्त करने के लिए किया गया था।

PLD के माध्यम से ६, १८ और ७० एनएम की अलग-अलग मोटाई की  $\alpha\text{-MoO}_3$  परतदार पतली फिल्म का संश्लेषण प्राप्त किया गया। सभी विकास मापदंडों को अनुकूलित किया गया था, और लेजर पल्स की संख्या को बदलकर तीन अलग-अलग मोटाई प्राप्त की गई थी। एक्स-रे-डिफ्रैक्शन (XRD) और रमन स्पेक्ट्रोस्कोपी ने अनिसोट्रोपिक  $\alpha\text{-MoO}_3$  के गठन की पुष्टि की। अटोमिक फोर्स माइक्रोस्कोपी (AFM) छवियों ने फिल्म की मोटाई में वृद्धि के साथ 2D परतों से उन्मुख क्रिस्टलीय विकास के लिए आकारिकी के विकास को दिखाया। एक्स-रे फोटोइलेक्ट्रॉन स्पेक्ट्रोस्कोपी (XPS) मापों में ७० एनएम पतली फिल्म नमूने में ऑक्सीजन रिक्तियों की उच्च सांद्रता और ६ एनएम मोटी २डी स्तरित नमूने में उच्च ऑक्सीजन सोखना दर्शाया गया है।  $\text{NO}_2$  गैस के प्रति मोटाई पर निर्भर गैस संवेदन व्यवहार का अध्ययन किया गया। 2D स्तरित नमूने ने कम तापमान (१०० डिग्री सेल्सियस ( $^{\circ}\text{C}$ )) पर लगभग २५% की उच्चतम प्रतिक्रिया दिखाई। इसने कम पता लगाने की सीमा (१०० ppb) और  $\text{NO}_2$  गैस के प्रति चयनात्मकता भी प्रदर्शित की। तुलनात्मक रूप से, TF ने १०० $^{\circ}\text{C}$  पर  $\text{NO}_2$  की ओर खराब

प्रतिक्रिया (४%) दिखाई, लेकिन २५०°C पर धीरे-धीरे बढ़कर ३५% हो गई, जो इसकी उच्च मोटाई के कारण विश्लेषण गैस के उच्च प्रसार का संकेत देती है।  $\alpha$ - $\text{MoO}_3$  फिल्मों की घटती मोटाई के साथ n-टाइप से p-टाइप गैस सेंसिंग रिस्पांस में बदलाव देखा गया, जो कम मोटाई वाले नमूने में धातु- $\text{MoO}_3$  जंक्शन पर बढ़ी हुई सतह सोखना और उच्च शोर्टकी बाधा के लिए जिम्मेदार हो सकता है।

PLD मापदंडों को अलग-अलग करके लंबवत और क्षैतिज रूप से उन्मुख  $\text{WS}_2$  स्तरित फिल्मों का संश्लेषण प्राप्त किया गया था। कम तापमान (४०० °C) और उच्च दबाव (७० mTorr) के संयोजन के साथ उगाए गए नमूनों ने ~ २-५ एनएम की परत मोटाई के साथ एक लंबवत परत जैसी वृद्धि प्रदर्शित की। हालांकि, उच्च तापमान (६०० °C) और कम दबाव (३० mTorr) पर, प्लानर फिल्म विकास प्राप्त किया गया था। XRD, रमन स्पेक्ट्रा और XPS स्पेक्ट्रा ने 2H अर्धचालक चरण और उच्च फिल्म गुणवत्ता की पुष्टि की। जबकि फील्ड एमिशन स्कैनिंग एलेक्ट्रॉन मिक्रोस्कोपी (FESEM), AFM और क्रॉस-सेक्शनल ट्रांसमिशन इलेक्ट्रॉन माइक्रोस्कोपी (TEM) मापों का उपयोग विकास तंत्र को स्पष्ट करने के लिए किया गया था। इसके अलावा, लंबवत उन्मुख फिल्मों ने कमरे के तापमान (RT) पर ५० ppb से कम पहचान की सीमा के साथ  $\text{NO}_2$  के प्रति चयनात्मकता के साथ सबसे अच्छी प्रतिक्रिया दिखाई। इसके विपरीत, प्लानर फिल्मों के मामले में दबी हुई प्रतिक्रिया प्राप्त हुई। परिणामों ने परत अभिविन्यास पर गैस संवेदन तंत्र और मापदंडों की एक बड़ी निर्भरता और किनारे की साइटों की महत्वपूर्ण भूमिका को दिखाया।

PLD के माध्यम से उच्च गुणवत्ता और अल्ट्राथिन  $\text{SnS}$  पतली फिल्म का संश्लेषण प्राप्त किया गया था, जिसके बाद गैस चरण संश्लेषण तकनीक का उपयोग करके महान धातु नैनोकणों (Ag, Au, और Pd) की सजावट की गई। कमरे के तापमान से ५०० °C के बीच विकास तापमान को बदलकर  $\text{SnS}$  फिल्म की वृद्धि को अनुकूलित किया गया था। प्रतिक्रिया और चयनात्मकता को ट्यून करने के लिए प्राचीन और धातु नैनोकणों से सजे  $\text{SnS}$  फिल्मों पर गैस सेंसिंग मापन किए गए थे।

गैस सेंसिंग मैकेनिज्म को और समझने के लिए, इन-सीटू गैस सेंसिंग तकनीकों को विस्तार से सेंसिंग मैकेनिज्म का पता लगाने के लिए नियोजित किया गया था।  $\text{Mo}$ -3d पीक की स्थिति और तीव्रता में परिवर्तन का विश्लेषण करके फिल्म की मोटाई, आकारिकी और  $\text{NO}_2$  गैस संवेदन के प्रभाव का अध्ययन करने के लिए  $\alpha$ - $\text{MoO}_3$  पतली फिल्मों पर नियर अम्बिएंट प्रेशर (NAP) XPS मापन किए गए थे। इन-सीटू केल्विन फोर्स माइक्रोस्कोपी (KPFM) प्राचीन, Ag और Pd नैनोपार्टिकल से सजाए गए  $\text{SnS}$  फिल्म पर किया गया

था। इन-सीटू KPFM ने विश्लेषण गैस के कारण फिल्म के कार्य समारोह में स्थानीय परिवर्तनों की मैपिंग की। NO<sub>2</sub> प्रतिक्रिया को बढ़ाने के लिए Ag का प्रभाव और H<sub>2</sub> गैस के प्रति चयनात्मकता बढ़ाने के लिए Pd का प्रभाव सतह की क्षमता और कार्य समारोह में परिवर्तन से प्रकट हुआ है। ये परिणाम २डी सामग्री के लिए संभावित संश्लेषण तकनीक के रूप में पीएलडी का पता लगाने के अवसर खोलते हैं और गैस सेंसर के रूप में उनके अनुप्रयोगों के लिए एक अद्वितीय परिप्रेक्ष्य देते हैं

# TABLE OF CONTENTS

---

---

CERTIFICATE .....	i
ACKNOWLEDGEMENTS .....	iii
ABSTRACT.....	vii
TABLE OF CONTENTS .....	xv
LIST OF FIGURES.....	xxi
LIST OF TABLES.....	xxxii
ABBREVIATIONS .....	xxxiii
Chapter 1 Introduction.....	1-1
1.1 History of 2D layered materials research.....	1-4
1.2 Basics of two-dimensional materials .....	1-5
1.2.1 Properties of 2D materials.....	1-5
1.2.2 Synthesis of 2D materials .....	1-9
1.2.3 Emerging applications .....	1-14
1.2.4 Challenges in the application of 2D materials.....	1-18
1.3 Material selection .....	1-20

1.3.1	2D transition metal oxide: Molybdenum trioxide ( $\alpha$ -MoO <sub>3</sub> ) .....	1-20
1.3.2	2D transition metal dichalcogenides: Tungsten disulphide (WS <sub>2</sub> ) 1-22	
1.3.3	2D transition metal monochalcogenides: Tin sulphide ( $\alpha$ -SnS)..	1-24
1.4	Applications of interest .....	1-25
1.4.1	Gas Sensors.....	1-25
1.4.2	Two dimensional materials for gas sensor .....	1-28
1.4.3	Operando and In-situ techniques to study the gas sensing mechanism .....	1-32
1.5	Objectives of the present work .....	1-35
1.6	Thesis overview .....	1-36
Chapter 2	Experimental and characterization techniques .....	2-1
2.1	Synthesis of 2D materials .....	2-3
2.1.1	Pulsed laser deposition technique .....	2-3
2.1.2	Thermal evaporation technique .....	2-6
2.2	Characterization techniques .....	2-8
2.2.1	X-ray diffraction technique.....	2-8

2.2.2	Raman Spectroscopy.....	2-11
2.2.3	Electron microscopy.....	2-14
2.2.4	X-ray Photoelectron Spectroscopy .....	2-19
2.3.2	Scanning Probe Microscopy .....	2-21
2.3.3	Electrical Characterization .....	2-26
2.3.4	Gas sensing measurements .....	2-27
Chapter 3 Thickness dependent evolution of structural, morphological and gas sensing properties of 2D $\alpha$ - MoO <sub>3</sub> thin films .....		
		3-1
3.1	Introduction .....	3-3
3.2	Experimental details.....	3-4
3.2.1	Growth of 2D $\alpha$ -MoO <sub>3</sub> layers and thin film using PLD technique	3-4
3.2.2	Material characterization techniques.....	3-5
3.3	Results and Discussion .....	3-5
3.3.1	Structural, morphological, and chemical properties of $\alpha$ -MoO <sub>3</sub> films	3-5
3.3.2	XPS analysis.....	3-9
3.4	Investigation of thickness dependent gas sensing properties .....	3-11

3.5	Mechanism of gas sensing .....	3-15
3.6	Conclusions .....	3-20
Chapter 4 Tailoring the vertical and planar growth of 2D WS <sub>2</sub> thin film using PLD for enhanced gas sensing properties .....		
4.1	Introduction .....	4-3
4.2	Experimental Details .....	4-4
4.2.1	Growth of vertical and planar WS <sub>2</sub> thin film using PLD technique 4-4	
4.2.2	Material characterization techniques.....	4-5
4.3	Results and Discussion .....	4-6
4.3.1	Structural, morphological, and chemical properties of WS <sub>2</sub> thin films 4-6	
4.3.2	XPS analysis.....	4-13
4.3.3	Investigation of growth mechanism of vertical and planar WS <sub>2</sub> thin film using cross sectional TEM and HAADF STEM .....	4-16
4.3.4	Gas sensing properties.....	4-22
4.4	Conclusions .....	4-30
Chapter 5 Metal nanoparticles decorated few layer 2D SnS film for enhanced room temperature gas sensing.....		
		5-1

5.1	Introduction .....	5-3
5.2	Experimental Details .....	5-4
5.2.1	Growth of 2D SnS thin film using PLD technique .....	5-4
5.2.2	Synthesis of Au, Ag, and Pd nanoparticles. ....	5-5
5.2.3	Material characterization techniques.....	5-6
5.3	Results and Discussion .....	5-7
5.3.1	Structural and Morphological analysis .....	5-7
5.3.2	XPS analysis .....	5-13
5.4	Gas sensing analysis .....	5-16
5.5	Mechanism of gas sensing .....	5-22
5.6	Conclusions .....	5-25
Chapter 6 Investigation of gas sensing mechanism in 2D layered materials		
using In-situ XPS and KPFM techniques .....		
6.1	Introduction .....	6-3
6.2	Experimental details.....	6-5
6.2.1	Near ambient pressure XPS setup.....	6-5
6.2.2	In- situ KPFM measurement setup.....	6-9
6.3	Near ambient pressure XPS of $\alpha$ -MoO <sub>3</sub> thin films .....	6-11

6.4 In-situ KPFM for gas sensing of pristine and metal nanoparticle decorated SnS thin films .....	6-15
6.5 Conclusion .....	6-20
Chapter 7 Summary, conclusions, and outlook .....	7-1
7.1 Summary and conclusions .....	7-3
7.2 Scope for future work .....	7-3
<b>REFERENCES</b> .....	R1
<b>APPENDIX</b> .....	A1
<b>PUBLICATIONS</b> .....	A6

## LIST OF FIGURES

---

Figure 1.1 Classification of nanomaterials based on degree of freedom. ....	1-3
Figure 1.2 Family of 2DMs based on their crystal structure.....	1-6
Figure 1.3 Top-down approaches to synthesise 2DMs. (a) Top-down approaches to synthesise 2D materials. (a) Mechanical exfoliation (b) liquid exfoliation (c) laser thinning, and chemical exfoliation. ....	1-10
Figure 1.4 Bottom-up approaches (a) Chemical vapour deposition (b) Hydrothermal synthesis (c) pulsed laser deposition, and (d) Molecular beam epitaxy.....	1-11
Figure 1.5 Application of 2D materials in electronics, photonics, spintronics, biosensors, catalysis, wearable technology, renewable energy, neuromorphic computing. (Adapted with the permission of Ref <sup>37-43</sup> .....	1-16
Figure 1.6 Images of (a) MoO <sub>3</sub> (b) WS <sub>2</sub> and (c) SnS crystal structure along different axis. ....	1-21
Figure 1.7 Typical response/recovery curve for a chemoresistive sensor. It shows change in the resistance of the sensor from R <sub>a</sub> to R <sub>g</sub> due to reaction with analyte gas and its resistance value recovers back after the removal of analyte gas. Response ( $\tau_{res}$ ) /recovery ( $\tau_{rec}$ ) time is also marked on the plot.	1-27
Figure 1.8 Pictorial literature survey indicating the major developments in the application of 2DMs in gas sensing. [The schematic has been reproduced with permission of Ref ] <sup>105,134-136,220,224,254,259-270</sup> .....	1-30
Figure 1.9 Schematic diagram describes the various In-situ/operando techniques for gas sensing. ....	1-33
Figure 2.1 Schematic diagram of the pulsed laser deposition setup. ....	2-4

Figure 2.2 Actual images of the PLD setup used for the synthesis of thin films.  
(a) PLD system for the deposition of MoO<sub>3</sub> thin film it includes a UHV chamber with a load lock setup and a KRF excimer laser (b) PLD system for the deposition of WS<sub>2</sub> and SnS thin film includes a HV chamber with an Nd:YAG laser. ....2-5

Figure 2.3 Schematic diagram of thermal evaporation system.....2-7

Figure 2.4 Diffraction of X-rays from parallel planes, depicting Braggs Law. ....2-8

Figure 2.5 Schematic diagram of the X-ray diffractometer. ....2-9

Figure 2.6 Raman scattering: Rayleigh, Stokes, and Anti-Stokes lines. ..2-12

Figure 2.7 Schematic diagram of Raman spectrometer. ....2-13

Figure 2.8 Schematic diagram of electron-matter interaction .....2-15

Figure 2.9 Schematic diagram of field emission scanning electron microscopy .....2-16

Figure 2.10 Schematic diagram of transmission electron microscopy.....2-18

Figure 2.11 (a) Schematic diagram of the basic X-ray photoelectron spectroscopy setup. (b) schematic describing of the XPS process showing the ejection of core level electron on the absorption of the X-ray photon. ....2-20

Figure 2.12 Schematic diagram of atomic force microscope (AFM) setup. 2-21

Figure 2.13 Energy level diagram of tip and sample with corresponding work function  $\phi_t$  and  $\phi_s$ . (a) Tip and sample without any electrical contact, showing the offset in their Fermi levels  $E_{ft}$  and  $E_{fs}$ , respectively. (b) Electrical contact between tip and sample results in the alignment of Fermi level via current flow and the offset in vacuum levels  $E_v$  is equal to VCPD (contact potential difference). (c) DC bias applied to nullify the VCPD. ....2-25

Figure 2.14 Electrical characterization setup consist of a probe station with Keithley sourcemeter 2400 and 6517A Electrometer.....	2-26
Figure 2.15 Schematic diagram of the gas sensing setup. ....	2-27
Figure 3.1 (a) XRD pattern for sample 2DF, UTF, and TF. The diffraction intensity for the (020), (040), and (060) peaks indicate preferentially oriented films along the [0k0] direction. (b) Raman spectra for sample 2DF, UTF, and TF indicate the formation of the $\alpha$ - phase of $\text{MoO}_3$ . ....	3-6
Figure 3.2 AFM investigation of the as-deposited $\alpha$ - $\text{MoO}_3$ films. Morphology plots of sample 2DF, UTF, and TF show the evolution of $\alpha$ - $\text{MoO}_3$ thin film with thickness. ....	3-8
Figure 3.3 XPS investigation of sample 2DF and TF (a) deconvoluted Mo 3d peaks of 2DF (b) deconvoluted Mo 3d peaks of TF (c) comparison of Mo 3d peaks of 2DF and TF (d) comparison of the VB maxima spectra of sample 2DF and TF. ....	3-9
Figure 3.4 XPS spectra of the O 1s peak of sample (a) 2DF and (b) TF, deconvoluted peak with higher intensity component showing lattice oxygen and the smaller shoulder component represents the adsorbed oxygen species. ....	3-11
Figure 3.5 (a) Comparison of sensing response vs. temperature to obtain optimal working temperature for 2DF, UTF, and TF towards $\text{NO}_2$ . (b) and (c) shows a comparison of sensing response vs. $\text{NO}_2$ concentration for sensors at 100 °C. Dynamic response curve of (d) 2DF, (e) UTF, and (f) TF towards 10 ppm $\text{NO}_2$ at their respective working temperature. ....	3-13
Figure 3.6 (a) Comparison of I-V plots of $\alpha$ - $\text{MoO}_3$ sample 2DF, UTF, and TF at 100 °C. (b) Energy band diagram of the sample 2DF with Ni/Au metal contacts and energy band diagram under bias in dry air and the presence of $\text{NO}_2$ mixed with dry air. ....	3-18

Figure 4.1. Optical images of as-grown WS<sub>2</sub> thin film with deposition parameters and sample notation. It depicts the variation in colour contrast of the WS<sub>2</sub> films at different growth parameters.....4-5

Figure 4.2. (a) XRD pattern for sample W1-W9. The diffraction intensity for the (002) peaks indicate preferentially oriented films along the [002] direction. (b) Raman spectra for sample W1-W9. Raman spectra peaks indicate the formation of the 2H-WS<sub>2</sub> phase. ....4-7

Figure 4.3 TEM investigation to study the effect of growth parameters on the structure and morphology of WS<sub>2</sub> film. TEM, HRTEM image in (a-d) correspond to samples W1, W3, W7, and W9, respectively. They depict the surface in two different magnifications. The left part shows the overall surface at lower magnification, whereas the right side show the high-resolution (HR) image. Image (e) and (f) represents the SAED pattern corresponding to sample W1 and W9, respectively. ....4-9

Figure 4.4 FESEM images of samples W1 – W9 indicates the morphological evolution of the WS<sub>2</sub> thin film with varying combination of deposition pressure (30–70 mTorr) and temperature (400–600 °C). The morphology varies from a planar growth in (a) W1 to a vertical growth in W9.. ....4-12

Figure 4.5 XPS investigation of sample W1, W3, W7 and W9 (a) Survey spectra of WS<sub>2</sub> thin films shows the various elements present and their chemical states. (b) Comparison of high resolution XPS spectra of W4f and S2p of sample W1, W3, W7 and W9. (c) W4f p peak is deconvoluted to W0, W4+, W6+ components. The deconvoluted components are compared in sample W1, W3, W7 and W9 showing the decrease in W0 component from sample W1 to W9 (d) Comparison of the VB maxima spectra of sample W1, W3, W7 and W9..4-14

Figure 4.6 FESEM images of as grown WS<sub>2</sub> film at 400 °C substrate temperature and 70 mTorr background pressure with (a) 100 (b) 250 (c) 500 (d) 1000 (e) 2000 laser pulse in each film. ....4-16

Figure 4.7 (a-b) FESEM images of as-grown WS<sub>2</sub> film at (a) 5 Hz, (b) 10 Hz laser frequency. (c-e) FESEM images of as-grown WS<sub>2</sub> film at (c) 120 mJ, (d) 90 mJ and (e) 70 mJ laser energy. Other growth parameters Substrate temperature, background pressure, and number of laser pulses is fixed at 400 °C, 70 mTorr, and 1000 laser pulses, respectively. ....4-17

Figure 4.8 (a – d) HAADF-STEM images of samples W1, W3, W7, and W9 showing the cross-sectional TEM of WS<sub>2</sub> on SiO<sub>2</sub>/Si substrates showing the variation in overall morphological structures of WS<sub>2</sub> thin films. High-resolution cross section TEM and HAADF images (e-h) shows a randomly oriented buffer layer followed by the preferential growth of vertical flakes. (i, k and m) shows the cross-sectional TEM images of sample W7, W3, and W1. The magnified HAADF images from the highlighted parts of images (j, i and n) reveals the out-of-plane to in-plane growth structures in samples W7, W3, and W1, respectively. ....4-20

Figure 4.9 (a–c) Schematic of the In-plane growth of WS<sub>2</sub> thin film. (a) Nucleation of layered nano-domains of WS<sub>2</sub>. (b) In plane growth of the film with impingement induced thinning preventing any preferential growth. (c) In plane grown WS<sub>2</sub> thin film. (d) Nucleation of randomly oriented nano-domains (e) Preferential growth of out of plane domains. (f) Out of plane grown WS<sub>2</sub> thin film. Here, the yellow- and turquoise-colored spheres represents the sulfur and tungsten, respectively. ....4-21

Figure 4.10 (a) Comparison of the I-V characteristics of sample W1, W7 and W9 at RT. (b) Sensing response vs. temperature for sample W1, W7 and W9 to obtain optimal working temperature for the sensors towards NO<sub>2</sub> (b) Sensing response vs. temperature for sample W1, W7 and W9 to obtain optimal working temperature for the sensors towards NO<sub>2</sub>. (c) Sensing response vs. time in sample W9 towards different concentration of NO<sub>2</sub> ranging from 2 ppm to 50 ppb. (d) Dynamic response curve showing the response vs. time plot towards 1ppm NO<sub>2</sub>. (e) Response/recovery time vs temperature plot towards 500 ppb NO<sub>2</sub>. (f) Histogram with the % response of

gases NO<sub>2</sub>, CO, NH<sub>3</sub> and H<sub>2</sub> for sample W9 showing selectivity towards NO<sub>2</sub> gas.....4-23

Figure 4.11 Effect of humidity on the sensing properties of sample W9 at two different RH values of (a) 20 % and (b) 70 % towards 1 ppm NO<sub>2</sub> at RT. (c) long term stability of the gas sensing performance in sample W9.....4-29

Figure 5.1 Integrated Schematic of gas phase synthesis setup to synthesize metal nanoparticles.....5-5

Figure 5.2 (a) XRD patterns for samples S1–S4. The diffraction intensity for the (040) peak indicate preferentially oriented films along the [0k0] direction. (b) RT Raman spectra (excitation wavelength: 514 nm) for samples S1–S5. (c) FESEM image of the as-grown SnS film at different temperatures showing the growth evolution with the substrate temperature. ....5-8

Figure 5.3 Evolution of SnS thin film by changing the number of laser pulse at 150 C substrate temperature (a) XRD patterns of SnS thin films with 5nm (S2\_150), 13nm (S2\_450) and 27nm (S2\_450) film thickness. (b) Raman spectra for SnS thin film with increasing film thickness. (c-e) FESEM image showing the morphological evolution of the SnS film. ....5-10

Figure 5.4 HRTEM images of as-grown Pd, Au and Ag nanoparticles showing the varying size. XRD, Raman spectra of the as-grown nanoparticles on the SnS film. FESEM images of metal nanoparticles decorate SnS thin film..5-12

Figure 5.5 XPS investigation of sample SnS, Pd\_SnS, Au\_SnS, and Ag\_SnS. (a) Survey spectra of SnS and metal nanoparticle decorated SnS thin films. (b) Comparison of high resolution PLD spectra of Sn3d and S2p peaks. (c, d) Deconvoluted high resolution spectra of Sn3d and S2p peaks. (e-h) High resolution spectra of Pd, Au and Ag. (h) Comparison of the VB maxima spectra.....5-13

Figure 5.6. (a) I-V characteristics of the SnS thin film with varying thickness. (b) Temperature dependent response towards 1ppm NO<sub>2</sub>. (c) Response vs NO<sub>2</sub>

concentration (d-f) Cyclic response towards different concentration of NO<sub>2</sub>. 5-17

Figure 5.7 Sensing performance of SnS, Ag\_SnS, Au\_SnS and Pd\_SnS samples (a) Comparison of the I-V characteristics at RT. (b) Response vs. temperature plot to obtain optimal working temperature (c) Sensing response vs NO<sub>2</sub> concentration ranging from 2ppm to 50 ppb. (d) sensing response vs. H<sub>2</sub> concentration for Pd\_SnS ranging from 70 ppm to 1 ppm. (e) Histogram with % response of gases NO<sub>2</sub>, CO, NH<sub>3</sub>, and H<sub>2</sub> for pristine and metal nanoparticles decorated SnS films to show the selectivity. (f-i) dynamic response curve showing the response vs time plot towards 2 ppm NO<sub>2</sub> in sample SnS, Ag\_SnS, and Au\_SnS, respectively and 70 ppm H<sub>2</sub> in Pd\_SnS. ....5-18

Figure 5.8 Response recovery time with the concentration of analyte gas in (a) SnS (b) Ag\_SnS (c) Au\_SnS and (d) Pd\_SnS. ....5-21

Figure 6.1 Schematic diagram of the ESCA beamline setup showing the optics involved to collimate and focus synchrotron X-ray beam onto the sample. 6-5

Figure 6.2 (a) Schematic diagram of the NAP cell (b) Actual images of NAP cell showing the pinhole and electrical feedthrough. (c) Inside image of NAP cell showing sample, electrical contact, and ceramic heater (d) NAP cell inside the chamber with gas line on the back. ....6-7

Figure 6.3 Schematic diagram of the Kelvin probe force microscopy (KPFM) setup. ....6-9

Figure 6.4 (a) Actual images of the KPFM setup (Bruker Multimode V) (b) a gas cell assembly to perform in-situ KPFM measurements in presence of desired gas. It has two luer fittings to insert and evacuate the analyte gas inside the cell.....6-10

Figure 6.5 (a) Comparison of Mo 3d peaks of sample 2D in vacuum vs mixture of NO<sub>2</sub> and NO gas (b) comparison of Mo 3d peaks of sample TF in vacuum vs

mixture of NO<sub>2</sub> and NO gas. VB maxima spectra of sample (c) 2D and (d) TF in vacuum and mixture of NO<sub>2</sub> and mixture of NO<sub>2</sub> and NO.....6-12

Figure 6.6 Ambient pressure XPS investigation of sample 2DF and TF (a) deconvoluted Mo 3d peaks of sample 2D in vacuum (b) deconvoluted Mo 3d peaks of sample 2DF in NO and NO<sub>2</sub> gas mixture (c) Comparison of the deconvoluted Mo 3d peaks of MoO<sub>3</sub> in vacuum and NO<sub>x</sub> (d) Mo3d peaks in NO<sub>x</sub> for the repeated five scans at the same position. ....6-13

Figure 6.7 In situ KPFM of SnS (a,b) Morphology image and KPFM map of the SnS sample in Ar (c,d) Topography image and KPFM map of SnS in NO<sub>x</sub> (e, f) Work function and surface potential values of SnS in Ar, NO<sub>x</sub> and Ar after NO<sub>x</sub> exposure. ....6-17

Figure 6.8 In-situ KPFM of Ag\_SnS (a,b) Morphology image and KPFM map of the Ag\_SnS sample in Ar (c,d) Topography image and KPFM map of Ag\_SnS in NO<sub>x</sub> (e, f) Work function and surface potential values of Ag\_SnS in Ar, NO<sub>x</sub> and Ar after NO<sub>x</sub> exposure. ....6-18

Figure 6.9 In-situ KPFM of Pd\_SnS (a,b) Morphology image and KPFM map of the Pd\_SnS sample in Ar gas (c,d) Topography image and KPFM map of Pd\_SnS in H<sub>2</sub> gas (e, f) Work function and surface potential values of Pd\_SnS in Ar, H<sub>2</sub> and Ar after H<sub>2</sub> exposure.....6-19

Figure A1 1 (a) Microscopic KPFM plots of the sample 2DF, UTF, and TF show spatial variation of the surface potential (b) Surface potential histograms corresponding to samples 2DF, UTF, and TF... ..... A1

Figure A1 2 (a)-(b) Dynamic response curve for sample 2DF, UTF and TF at 200 °C towards 10 ppm NO<sub>2</sub>.....A2

Figure A2 1 (a) XRD pattern for sample W1-W9 indicates small intensity diffraction peaks corresponding to (101) planes present in only sample W9. (b) XRD pattern of the WS<sub>2</sub> film grown at 10 mTorr background pressure and 600 °C substrate temperature..... A4

Figure A2 2 AFM images of the as-grown WS<sub>2</sub> film, each with 100 laser pulses at different Argon pressure.....A5

Figure A3 1 The HRTEM images of palladium, gold and silver nanoparticles deposited directly on the TEM grid using IGPS setup. The deposition time in all three case is kept 30 min with 60Hz spark frequency and sintering temperature of 800 °C for Pd nanoparticles 500 °C for Au or Ag nanoparticles. (a-f) TEM images at two magnification indicates the uniform distribution of spherical nanoparticle with bigger agglomerates in Pd. Comparatively smaller agglomerates with highest particle density is observed in Au. Whereas, Ag has minimum agglomeration with uniform particles distribution. (g-f) Corresponding SAED pattern are used to find the d spacing in all three particles which matches well with the corresponding XRD data.....A6

## LIST OF TABLES

---

---

Table 1-1 Table comparing of the various synthesis techniques used to fabricate 2DMs adapted with the permission of Ref no. 26.....	1-12
Table 5-1 Peak position of the deconvolute Sn 3d and S 2p peaks. ....	5-15
Table 6-1 Comparison of the characteristic deconvoluted Mo 3d peaks from ambient pressure XPS spectra of sample 2DF in vacuum and in gas mixture of NO and NO <sub>2</sub> .....	6-14
Table A1 The response and recovery time for 2DF, UTF and TF towards 10 ppm NO <sub>2</sub> at 100 °C and 200 °C. ....	A2

## ABBREVIATIONS

---

DOS	Density of states
vdW	van der Waals
MBE	Molecular beam epitaxy
XRR	X-ray reflectivity
XRD	X-ray diffraction
FESEM	Field electron scanning electron microscopy
XPS	X-ray photoelectron spectroscopy
B.E.	Binding energy
MFC	Mass flow controller
2D	Two dimensional
3D	Three dimensional
EDX	Electron diffraction analysis
TEM	Transmission electron microscopy
HRTEM	High-resolution transmission electron microscopy
AFM	Atomic force microscopy
TMD	Transition metal dichalcogenides
SC	Surface charge
SPM	Scanning probe microscope
PSPD	Position-sensitive photodetector
PECVD	plasma-enhanced chemical vapor deposition
JCPDS	Joint Committee on Powder Diffraction Standards
BSE	Backscattered electron
PLD	Pulsed laser deposition
IGPS	Integrated gas phase synthesis setup
PVD	Physical vapour deposition
PVA	Polyvinyl alcohol
KrF	Krypton flouride
EDS	Energy dispersive spectrometer
CB	Conduction band

VB	Valance band
SP	Surface potential
KPFM	Kelvin probe force microscopy
CCD	Charge coupled device
LOD	Limit of detection